PCCP

PAPER

View Article Online
View Journal | View Issue

Cite this: *Phys. Chem. Chem. Phys.*, 2025, **27**, 21214

Investigation of methyl-vinyl ketone, 2- and 3-butenal decomposition pathways through semi-automated variable reaction coordinate transition state theory

Andrea Della Libera and Carlo Cavallotti *

The reactivity of unsaturated aldehydes and ketones is of interest both in combustion, as they are formed as intermediate species in the oxidation of biofuels, as well as in atmospheric chemistry, as they appear as intermediate products in the oxidation of alkenes, such as isoprene. In this work we investigate the reactivity of the simplest unsaturated aldehydes and ketones, namely methyl vinyl ketone (MVK), 2-, and 3-butenal (2- and 3-BUT), on the C_4H_6O singlet potential energy surface (PES). An important part of this study is the accurate determination of rate constants for the seven major barrierless decomposition channels: the bond fissions of MVK to (1) $CH_2CHCO + CH_3$ and (2) $CH_3CO + C_2H_3$, the bond fissions of 2-BUT to (3) $CH_3CHCH + HCO$, (4) $CHCHCHO + CH_3$ and (5) $CH_2CHCHCHO + H$, and the bond fissions of 3-BUT to (6) $CH_2CHCH_2 + HCO$ and (7) $CH_2CHCHCHO + H$. Rate constants were determined using variable reaction coordinate transition state theory (VRC-TST), as implemented in EStokTP, through the extensive use of automated procedures to exploit both single and multireference methodologies and to semi-automatically carry out the determination of minimum energy paths, the evaluation of geometric and high level correction potentials, and the definition of the pivot points necessary to construct the dividing surfaces. As a result of this investigation, we propose a novel mechanism for the decomposition of 2-butenal to carbon monoxide and propene, involving isomerization to 3-butenal through two keto–enol tautomerization steps. Rate constants for both the dissociation and the reverse recombination pathways, as well as for the whole PES are determined for all the investigated pathways by integrating the master equation as a function of temperature and pressure, finding a good agreement with available experimental data, and are reported in a format suitable to be used both for atmospheric and combustion kinetic simulations.

Received 9th May 2025,
Accepted 8th September 2025

DOI: 10.1039/d5cp01744k

rsc.li/pccp

1. Introduction

The comprehension of the reactivity of unsaturated aldehydes and ketones is important in combustion as it plays an important role in the oxidation of some important biofuels, where they are formed as intermediate decomposition products.[1–3] Unsaturated aldehydes and ketones have also been observed as products in the atmospheric oxidation of alkenes.[4] Despite this, only a few studies have been dedicated to the investigation of the kinetics of these systems, in part because of the difficulty of estimating accurate rates of the many barrierless reaction channels ruling their reactivity. The present work has the aim of using a recently developed computational methodology to investigate the decomposition kinetics of the simplest unsaturated aldehydes and ketones: 2-butenal (crotonaldehyde, 2-BUT), 3-butenal (3-BUT), and methyl vinyl ketone, which are all C_4H_6O isomers.

The reactivity of MVK, the lowest energy C_4H_6O isomer among those investigated here, has been the subject of several studies. MVK is among the main decomposition products of cyclohexanone, whose decomposition mechanism was studied by Porterfield *et al.*[5] Both MVK and its corresponding enol were identified with photoionization mass spectroscopy and matrix infrared absorption spectroscopy. Cyclohexanone decomposition could be interpreted only including the fragmentation of MVK by loss of H and CH_3 in the main reaction steps. Also, the 0 K heats of formation for both *cis* and *trans* MVK conformers were determined using a theoretical HEAT like approach[6–8] and isodesmic reactions, obtaining results in agreement with previous investigations.[9] The relevance of enols as intermediates in combustion was proposed by Taatjes *et al.*,[10] while the existence of the keto–enol tautomerization pathway for this specific system was recently proved by Couch *et al.*[11] Since MVK

Dipartimento di Chimica, Materiali e Ingegneria Chimica, Politecnico di Milano, 20131 Milano, Italy. E-mail: carlo.cavallotti@polimi.it

atmospheric kinetics plays an important role in isoprene decomposition, its photoisomerization and decomposition pathways were recently investigated theoretically by So *et al.*[12] In their analysis of the ground state MVK potential energy surface (PES), which included both isomerization and dissociation pathways, a total of six wells, six fragmentation products, and 14 reaction channels were identified. The most relevant decomposition channels are two barrierless decomposition reactions, leading to CH_3 + CH_2CHCO (1-oxoprop-2-enyl) and C_2H_3 + CH_3CO (acetyl), and molecular dissociation to C_2H_4 + CH_2CO. Tautomerizations to 2-hydroxybutadiene (HBD) and 1-hydroxymethylallene were reported. The former is the favoured product of isomerization. Cyclization reactions, such as formation of 2-methyloxetene from MVK and cyclobutanone from 2-HBD, were also described, though their formation requires overcoming significant energy barriers.

The decomposition kinetics of two other C_4H_6O isomers, 2-butenal and 3-butenal, has recently attracted interest in combustion. These species were in fact found as reactive intermediates in several cycloalkyl reactions with $O(^3P)$[13–16] and can be present in relevant concentrations in bio-oils.[17] The high temperature decomposition of 2-BUT and its product distribution was studied by Lifshitz *et al.*[18] Two bond cleavages to CH_3 + CHCHCHO (3-oxo-1-propenyl) and HCO + CH_3CHCH (1-propenyl), and H migration resulting in CO + C_3H_6 (propene) were proposed to be the main initiation pathways for decomposition. The latter reaction presents a well-defined transition state and can be considered a quencher in combustion systems, as also suggested by Chabán *et al.*,[19] who experimentally studied 2-BUT decarbonylation in the 653–763 K and 55.5–150 Torr ranges. Erastova *et al.*[20] followed this lead and carried out a theoretical investigation of possible elimination mechanisms at the B3LYP and MP2 levels, estimating energies at the MP4 level. They proposed two pathways for 2-BUT decarbonylation: a single step concerted mechanism and a two-step mechanism that involves hydrogen migration followed by CO elimination. 3-BUT has been recently found among the decomposition products of furan,[21] which motivated the recent study of H-abstraction reactions by atomic hydrogen on 3-BUT performed by Passos *et al.*[22]

The reactivity on the C_4H_6O PES is of interest for the atmospheric, combustion, and astrochemical kinetic communities as it is accessed following the addition of atomic oxygen in its ground state to 1,3-butadiene and 1,2-butadiene, which are the simplest unsaturated conjugated alkenes, and the successive fast intersystem crossing (ISC) to the singlet PES. It occupies therefore a relevant place in the vast class of $O(^3P)$ reactions,[23] which we investigated systematically in the last years.[24–30] In particular, it is known that $O(^3P)$ addition is one of the most sensitive reactions in 1,3-butadiene oxidation.[31,32] The modeling of its reactivity however is hampered by a lack of knowledge concerning the branching fraction (BF) among the many possible reaction products. Recently we investigated the reactivity on the 1,3 C_4H_6 PES, as accessed following $O(^3P)$ addition, using rate constants calculated in the present work.[33] A similar publication is in preparation for the reactivity of $O(^3P)$ with 1,2-butadiene.

The theoretical study of the reactivity of these molecules is complicated by the need to investigate at a suitable level of accuracy the related singlet potential energy surfaces (PESs). This is often a challenging task[34,35] for at least two reasons. First, because it is necessary to determine a complete map of all stationary points that are relevant to the description of the specific portion of the PES that is under investigation. As it is difficult to prove that the search is complete, several automated methodologies to explore PESs have been proposed in the last few years to address this issue.[36–40] This investigation is even more complicated on singlet PESs, as some wells may be connected by saddle points that have diradical nature, which is badly described by black box, computationally efficient single reference *ab initio* theoretical methods routinely adopted to investigate PESs, such as density functional theory (DFT). The second motivation that further complicates singlet PES investigations is that usually the fastest exit (or entrance) channels are barrierless. In these cases, rate constants can be determined either through dynamic trajectory calculations, which require high quality multidimensional PESs to be predictive, or using a variational form of transition state theory (TST). The latter, whose most advanced version is variable reaction coordinate transition state theory (VRC-TST), requires if precision is desired the use of multireference *ab initio* methods.[1,41,42] In this context, the approach we followed in investigating the reactivity on the C_4H_6O PES in the present work consisted in the systematic investigation of all the isomerization reactions that can be accessed by the MVK, 2-BUT, and 3-BUT wells, followed by the determination of the rate constants of the less endothermic homolytic decomposition pathways. In this last step we extensively used our recent partially automated protocol to compute rate constants using VRC-TST. This allowed us to estimate efficiently and accurately rate constants for seven barrierless reaction channels active on the C_4H_6O PES.

This paper is organized as follows. In Section 2 the computational method used in this work are described in detail. A brief description of the adopted VRC-TST protocol, which has been implemented in EStokTP and is therefore available as open-source software (**https://github.com/EStokTP/EStokTP**),[43] is reported as well in this section. The simulation results are discussed in Section 3, where they are also compared to the available experimental data.

2. Methods

The reactivity on the C_4H_6O PES was investigated using the *ab initio* transition state theory-based master equation (AI-TST-ME) method.[34] Details on the application of this approach to the specific system here investigated are reported in the following three sub-sections.

2.1 *Ab initio* calculations and PES investigation

Structures, gradients, and Hessians of stationary points (both wells and saddle points) on the C_4H_6O PES were determined at the ωB97X-D/aug-cc-pVTZ level of theory. Preliminary

explorations of the PES were performed using the 6-311+G(d,p) basis set. A conformational analysis was also carried out by contextual random rotations of all torsional dihedral angles for each investigated well to identify the minimum energy conformer. All calculations were performed using an ultrafine grid (99 590 integration points per atom). Energies were evaluated at the CCSD(T)/aug-cc-pVTZ level and extrapolated to the complete basis set limit (CBS) as suggested by Martin,[44] using density fitted MP2 energies computed with the aug-cc-pVQZ and aug-cc-pVTZ basis sets. Energies were then corrected for the correlation of core electrons computing the difference between CCSD(T,core)/cc-pcVTZ and CCSD(T)/cc-pVTZ energies. When T1 diagnostics exceeded 0.025, energies were determined at the CASPT2/aug-cc-pVTZ level. This was the case for the transition states connecting 3-BUT and the vinyl oxirane species VO (TS01), VO and MVK (TS05), and MVK to the decomposition products CH_2CO + C_2H_4 (TS07). Also the TS between 3-BUT and its enol tautomer BD (TS02), despite the small T1 diagnostic (0.017), was investigated at the CASPT2 level, as it plays an important role in decomposition kinetics of 2-BUT and it was thus important to investigate whether it could have a relevant multireference character. All CASPT2 calculations were performed using ωB97X-D geometries, determined using an unrestricted formalism with wave functions computed with a broken symmetry guess. The selection of the most suitable active spaces (AS) was performed at the CASSCF/cc-pVDZ level, using then the determined wavefunction as guess for successive CASSCF/aug-cc-pVTZ and CASPT2/aug-cc-pVTZ level calculations. A shift of 0.2 was used for all CASPT2 calculations. All CASPT2 energy barriers were computed performing two distinct calculations at the same level of theory to ensure consistency, one for the saddle point and one for the reference well. The AS used in the multireference calculations are summarized in Table 1 together with the well with respect to which energy barriers were computed. Particular care was placed in inspecting the orbitals of saddle points and wells to ensure consistency in the AS selection.

Partition functions of internal rotations were calculated using the 1D hindered rotor (1DHR) model implemented in MESS.[45] Torsional potentials were computed at the same level of theory used for geometry optimization. Methyl groups were always treated as 1DHRs. MVK and 2-BUT present a second rotor, in which CHO and C_2H_3 are the rotating moieties, respectively, and 3-BUT presented 2 additional rotors, with CHO and C_2H_3 as the rotating groups. For VO, and $CH_2CHCHCHO$, only one rotor was considered, the C_2H_3 rotating top. Tunneling corrections were evaluated using the Eckart model.

2.2 Rate constant estimation and variable reaction coordinate transition state theory

Pressure-dependent rate constants were computed in the 300–2500 K temperature and 0.1–100 atm pressure ranges solving the one-dimensional multi-well master equation (ME) using the MESS solver.[45] Collisional energy transfer parameters were computed in Ar bath gas as suggested by Jasper[46] using the correlations provided for alcohols, as unsaturated aldehydes were not parameterized. The single exponential down model energy transfer parameter so determined is $\langle \Delta E \rangle = 395(T/300)^{0.49}$ cm^{-1}, while the collisional frequencies for all wells were estimated using the Lennard-Jones model with $\sigma = 4.21$ Å and $\varepsilon = 331$ K.

Rate constants of reactions which involve a well-defined saddle point were determined using conventional TST, while those of barrierless channels were estimated with VRC-TST, which is the state of the art theory for the evaluation of rate constants for this reaction class. In VRC-TST, rate constants are evaluated by directly counting the density of states (DOS) of the transition state over dividing surfaces constructed over pivot points placed in proximity of the reacting centres. Only the degrees of freedom (DOF) describing the relative orientation of the fragments, usually referred to as transitional DOFs, are considered in the DOS evaluation, while the geometry of the fragments is kept frozen. One of the main advantages of VRC-TST is the proper and computationally efficient evaluation of the DOS for the transitional DOFs that, being large amplitude motions, are highly anharmonic. This evaluation is performed through stochastic integration determining single point energies (SPE) through on the fly multireference calculations. More details on the implementation of VRC-TST are reported in literature reference publications.[41,48]

VRC-TST calculations were performed for seven barrierless reactions, namely decomposition of MVK to CH_2CHCO + CH_3 and CH_3CO + C_2H_3, decomposition of 2-BUT to CH_3CHCH + HCO, CHCHCHO + CH_3 and $CH_2CHCHCHO$ (1-oxo-*n*-butadienyl) + H, and decomposition of 3-BUT to CH_2CHCH_2 (allyl) + HCO and $CH_2CHCHCHO$ + H. The minimum energy paths (MEPs) of each bond fission reaction were evaluated as a function

Table 1 Active spaces used in multireference calculations and wells relatively to which energy barriers were computed (in parentheses)

Stationary points	Active space
TS01 (VO)	**(14e,13o):** (2e,2o) π and π* CC bond; (4e,4o) 2 σ and σ* CO bonds for the reactant and 1 σ and σ* CO bond plus 2 radical centers for the TS; (2e,2o) σ and σ* CC bond; (4e,4o) 2 σ and σ* CH bonds; (2e,1o) lone pair of O.
TS02 (3-BUT)	**(10e,9o):** (2e,2o) π and π* CC; (2e,1o) lone pair of O; (2e,2o) σ and σ* CO bond; (4e,4o) σ and σ* CH bond and π and π* CO bond for the reactant, σ and σ* OH bond and π and π* CO (deformed) bond for TS.
TS05 (VO)	**(14e,13o):** (2e,2o) π and π* CC bond; (4e,4o) 2 σ and σ* CO bonds for the reactant and 1 σ and σ* CO bond plus 2 radical centers for the TS; (4e,4o) 2 σ and σ* CC bonds; (2e,2o) σ and σ* CH bond; (2e,1o) lone pair of O.
TS07 (HBD)	**(10e,10o):** (4e,4o) 2 π and π* CC bonds for reactant, 1 π and π* CC bond and 2 radical centers for TS; (2e,2o) σ and σ* CO bond; (2e,2o) σ and σ* CH bond for the reactant, OH bond for the TS; (2e,2o) σ and σ* central CC bond.

of the breaking bond length with a step of 0.2 Å in the 1.8–4.0 Å range.

Reaction fluxes were determined over multifaceted dividing surfaces performing both short range and long range simulations. For the former, spherical dividing surfaces were generated using pivot points positioned along the vector connecting the atoms whose bond is breaking, while in the latter they were placed on each fragment centre of mass. Microcanonical reaction fluxes were then minimized over an ensemble of dividing surfaces constructed varying the distance between the pivot points which, in short range simulations, were initially placed on the reacting atoms and then displaced by 0.1 and 0.3 bohrs along the direction of the molecular bonding orbital being broken in the reaction. The distance between pivot points was varied between 2.5 and 10.0 bohrs for short range simulations, and between 10.0 and 20.0 for long range simulations. Reactive fluxes were computed through stochastic sampling with a 5% convergence threshold, taking a minimum of 200 points for each surface and multiplying by a factor 0.9 to account for dynamical recrossing effects, as described for example by Lupi.[47] SPEs were computed as a function of the fragment orientation using stochastic sampling at the CASPT2 level using the cc-pVDZ basis set and a minimal (2e,2o) active space. Fragment geometries, which are frozen in all VRC-TST calculations, were determined at the CASPT2/cc-pVDZ level of theory. Energies obtained in the Monte Carlo (MC) sampling were corrected to account for the low level of theory employed and geometry relaxation through the introduction of a distance dependent potential computed as:

$$E_{\text{VRC-TST}} = E_{\text{MC}} + \Delta E_{\text{en}} + \Delta E_{\text{geom}} \quad (1)$$

In eqn (1), E_{MC} is the energy obtained for a single MC sampling point. ΔE_{en} is defined as the difference between CASPT2(6e,6o)/aug-cc-pVTZ and CASPT2(2e,2o)/cc-pVDZ energies calculated on MEP geometries, which were obtained through constrained optimizations performed at the CASPT2(6e,6o)/cc-pVDZ level at fixed fragment separation. The (2e,2o) AS included the electrons involved in the breakage of the bond between the fragments and their bonding and antibonding orbitals, while the (6e,6o) AS always included the radical orbitals, and the C–C and C–O π bonding and antibonding orbitals. ΔE_{geom} was computed as the energy difference between MEP optimized geometries and geometry optimizations performed using frozen fragment geometries at the same level of theory. Thus only five degrees of freedom are optimized, corresponding to the variables that define the orientation of one fragment with respect to the other, namely two angles and three dihedral angles. All CASPT2 energies computed for VRC-TST calculations were used to determine interaction energies between two reacting fragments, whose energy was evaluated with eqn (1) with a distinct calculation, in which a restrained geometry optimization was performed at the CASPT2(6e,6o)/cc-pVDZ level of theory with the distance between the fragments kept fixed at 10 Å.

The VRC-TST protocol was carried out using VaReCoF,[41,48,49] which in turn relies on Molpro[50,51] for MC sampling and multireference calculations. The scan of the MEP and the preparation of the input files necessary to VaReCoF were performed with a semi-automatic protocol implemented in a modified version of EstokTP, as described in detail in the following section.

2.3 VRC-TST semi-automatic protocol

2.3.1 Protocol overview. The EStokTP protocol for VRC-TST is organized in a series of steps that can in principle be executed automatically and sequentially without human intervention once a set of input files are defined, as summarized in Fig. 1. At the present state of implementation however few decisions and checks from the user are still necessary, as discussed in the following. Here we present an overview focused on the strategy of the protocol, while in the next section we report implementation details. The starting point (step 0) are the optimized geometries, frequencies, and high-level (HL) energies of the reactant and the two radical fragments that are the products of the reaction. Then, a reference point along the MEP is selected and the whole system (made up of the fragments at fixed distance) is optimized at the chosen level of theory (step 1). The geometry obtained is in turn used as a reference for optimizing further geometries at different fixed fragment distances along the MEP (step 2). Energies along the MEP are computed using a multireference approach, using an AS that includes all orbitals that are directly or indirectly involved in the bond formation/breakage process (usually the breaking bond, all π orbitals, their respective anti-bonding orbitals, and relevant lone pair electrons with their orbitals). The analysis of the MEP is a bottleneck for the process, since it is not guaranteed that the AS guess automatically generated will include the desired orbitals both in step 1 as well as throughout the calculations. Thus, a manual check on the orbitals included in the AS is at present required. EStokTP has at this point enough information to perform VTST calculations using the rigid rotor harmonic oscillator (RRHO) approximation both for the recombination and the inverse decomposition reactions, using multireference energies to determine MEP energies for the recombination reaction and 0 K HL enthalpy changes for the decomposition reaction (step 3). To proceed with the VRC-TST protocol, it is necessary to compute correction potentials for all the points along the MEP for the geometry (ΔE_{geom}) and the energy (ΔE_{en}) (step 4). The former requires an optimization of each MEP point with the fragments placed at fixed distances using the geometry optimized for the successive VRC-TST calculations. Only the five coordinates that determine the relative positions of the fragments are optimized (these become two or four degrees of freedom in the case of atomic or biatomic fragments, respectively). The computation of ΔE_{en} requires a single point energy calculation on MEP geometries at the level of theory of the successive VRC-TST calculations. Apart from the manual checks on the AS consistency, all the steps aforementioned are automatically performed by EStokTP and lead to the creation of the input files used by VaReCoF for the VRC-TST computations (step 5).

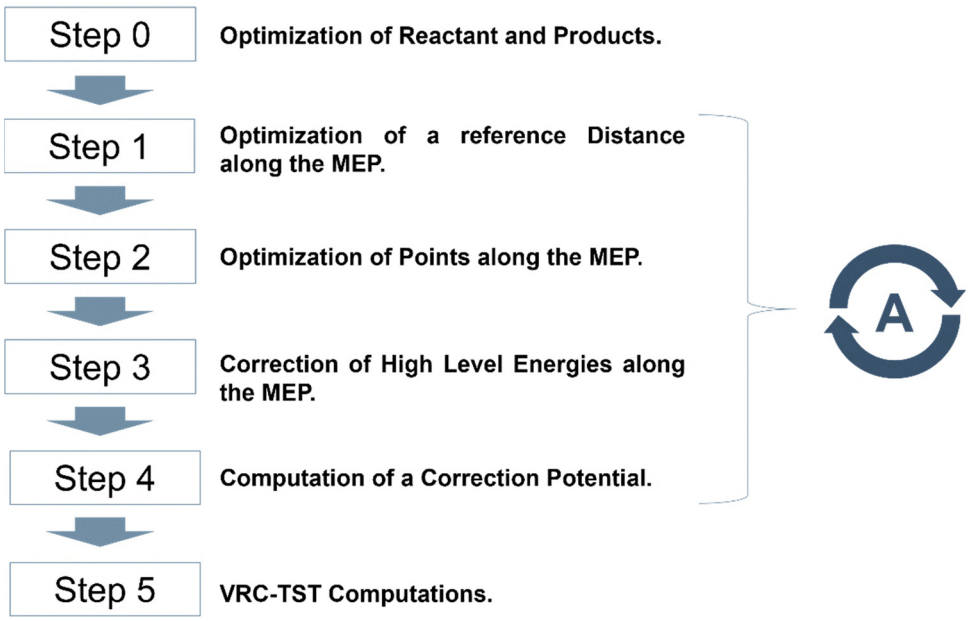

Fig. 1 Scheme of the semi-automatic protocol implemented in EStokTP for preparing and running VRC-TST calculations with VaReCoF. Initially, reactant and products are optimized with black box single reference methods, then the MEP is analysed by optimizing the fragments at fixed distances with a multireference approach. The energies are corrected to account for the different levels of theory of the 0 K HL enthalpy change computed for reactant and products, a step necessary for VTST computations. Then, the correction potential, accounting for both the different level of theory between the MEP scan and the MC sampling and the geometry relaxation of the fragments at different distances is computed. Finally, MC sampling for determination of the minimum reaction flux is performed.

2.3.2 Implementation. The steps of the protocol implemented in EStokTP to prepare and carry out VRC-TST calculations are summarized in Fig. 2.

In step 0 all the information necessary to run the protocol are generated and the level of theories for the different steps of the calculations (LOT) and the Z-matrix of reactant and products are defined. Both reactant and products are optimized at a suitable LOT, ωB97X-D/aug-cc-pVTZ in this work, with HL energies computed at the CCSD(T)/aug-cc-pVTZ level and extrapolated to the CBS as described in Section 2.1. Frequencies are determined at the same level used for the geometry optimization. The geometries of the two fragments are also optimized at the same LOT used for the MEP simulations, CASPT2/cc-pVDZ for the present system. The sum of the electrons and orbitals included in the AS of the two fragments is used as guess for the successive calculations.

Step 1 determines the first reference point along the MEP initially creating a Z-matrix using information on the connectivity from the step 0 reactant and performing a low level DFT optimization (ωB97X-D/6-311+G(d,p)). Then, it generates a guess for the AS of the MEP structure and uses it to run a multireference optimization (at the CASPT2/cc-pVDZ level in this work). Finally, the energy is computed at the same LOT increasing the basis set to aug-cc-pVTZ.

Step 2 is the repetition of the previous step for additional fixed fragment distances along the MEP. The guess structure is taken as the one optimized in step 1 by modifying the distance between the fragments. The guess for the AS is once again generated from the AS of the isolated fragments. The optimization and single point calculation on the fragments at 'infinite' distance (usually simulated with fragments placed at 10 Å) is also carried out. A human check of the automatically selected orbitals, usually performed through direct visualization, is generally recommended.

Step 3 allows to run an optional VTST calculation in the RRHO approximation, which is not mandatory for the subsequent VRC-TST work but allows to compare the two approaches. The energies computed along the MEP are referred to the reactants using the 0 K reaction enthalpy change computed in step 0.

Step 4 determines the correction potential at the LOT described in Section 2.2. For each point along the MEP one further optimization is performed at the same LOT of Step 2. Only up to five transitional coordinates are optimized, while the fragments geometries are fixed to those determined at the CASPT2 level in step 0. Successively, SPE multireference calculations are performed on Step 2 geometries at the LOT employed for the MC sampling to determine the 'high level' energy correction for the potential (the ΔE_{en}. term of eqn (1)). For the fragments at 'infinite' distance, a further energy calculation is performed, with the fragment geometries frozen as done to compute the geometry correction, using the coordinates that define the relative position of the fragments taken from step 2 at 'infinite' distance, but using the structures determined at the same LOT that will be used for the VRC-TST calculations (CASPT2/cc-pVDZ per the present system). This energy will be the reference to compute relative energies in the SPE estimates performed by VaReCoF in the stochastic

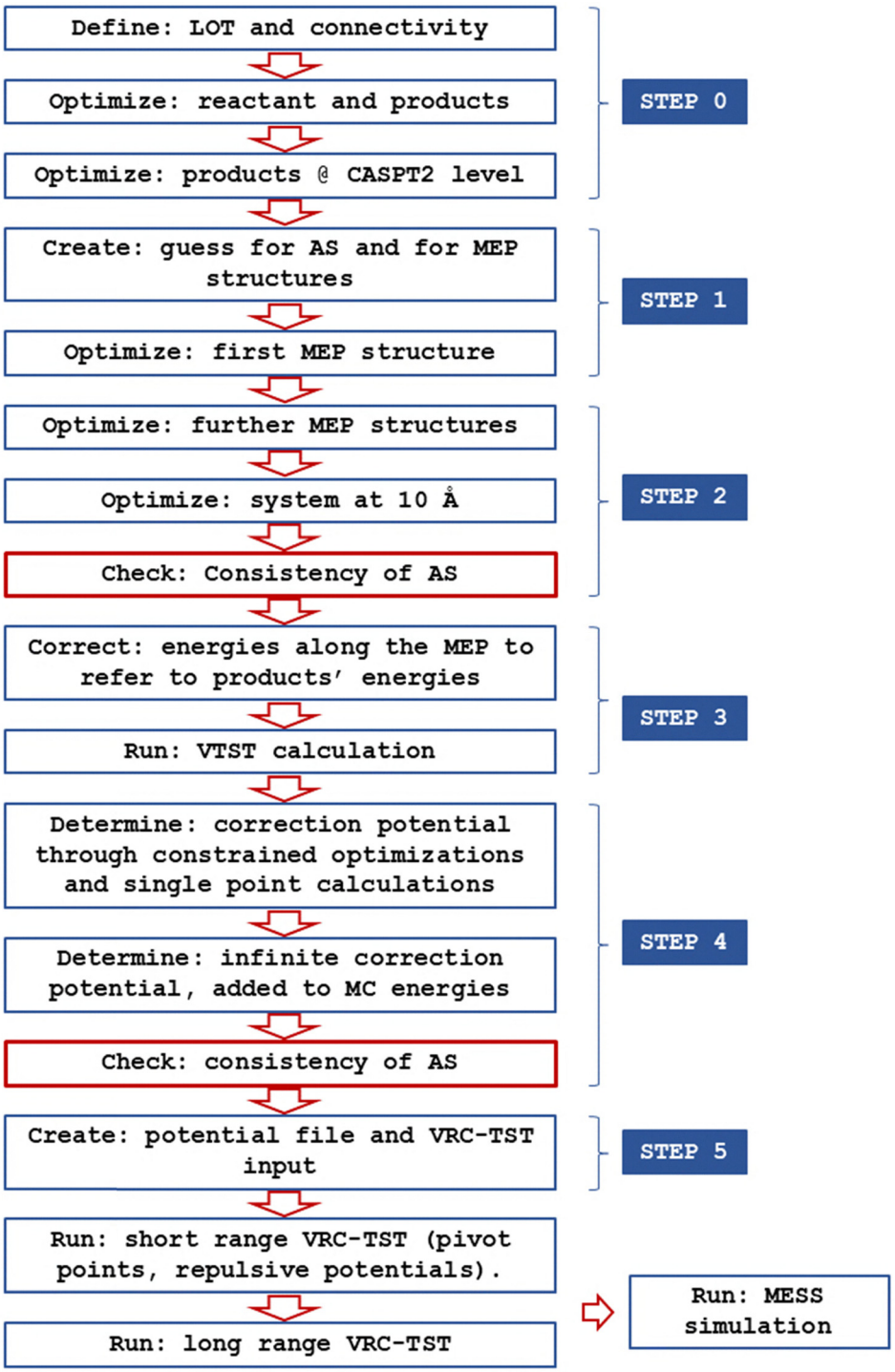

Fig. 2 Block diagram of the semi-automatic protocol implemented in EStokTP to prepare and run VRC-TST calculations.

sampling. Once again, a check on the consistency of the AS is recommended.

Step 5 collects all information generated in previous steps and generates the VRC-TST working directory, in which all input files are collected, including the geometries of the fragments, the number and positioning of the pivot points, and the distance dependent correction potential. Two subfolders are generated to differentiate between short and long-range calculations. For short range computations, the pivot points are placed on or in proximity of the dissociating atoms, and it is possible to add additional pivot points or repulsive potentials between specific atoms to avoid the influence of secondary reaction pathways in the determination of the reactive flux. As a default, multifaceted dividing surfaces with spherical surfaces

generated using radii between 4.5 and 10.0 bohrs are used. For long range calculations, the pivot points are placed on the centres of mass of the fragments and distances between 10 and 20 bohr are explored. A reference geometry along the MEP, 2.4 Å in this work, was used to characterize a direction vector for the breaking bond and thus the positions of the pivot points on each fragment. VaReCoF simulations can now be run and finally the short and long range microcanonical energy resolved fluxes can be computed and used to run multi-well master equation simulations with MESS, thus obtaining temperature and pressure dependent phenomenological rate constants.

3. Results and discussion

The presentation of the results and the discussion of the investigation of the reactivity on the C_4H_6O PES is organized as follows. First, the main isomerization pathways between MVK, 2-BUT, and 3-BUT are discussed. Interestingly, this is the same portion of the C_4H_6O PES that determines the reactivity on the singlet PES in the reaction between $O(^3P)$ and 1,3-C_4H_6. As this PES was used in our previous study of $O(^3P)$ + 1,3-C_4H_6,[33] we dedicate part of the discussion to this aspect. The successive sections examine and discuss the decomposition pathways of MVK, 2-BUT, and 3-BUT. Phenomenological rate constants were computed through ME simulations performed over the full PES described in the following, comprehensive of the isomerization pathways described in Section 3.1 and the decomposition pathways of Sections 3.2–3.4. All rate constants computed in this work have been fitted in the PLOG format after having being post processed using the MEL approach[52] to lump the BD and 2-BUT species in a unique well, and are reported as the SI to this paper.

3.1 Isomerization pathways on the C_4H_6O PES

The main isomerization pathways explored in the present work are summarized in Fig. 3. The three most stable wells are those whose reactivity is under investigation: MVK, 2-BUT, and 3-BUT. Isomerization of vinyl-oxirane (VO) to MVK requires overcoming an energy barrier of 57.8 kcal mol^{-1}. The TS that connects VO to MVK, TS05, has strong multireference character (0.097 T1 diagnostic). This is indirectly confirmed by the fact that energy barriers computed using single reference wavefunctions change significantly with the level of theory, going from the 58.8 kcal mol^{-1} computed at the ωB97X-D/aug-cc-pVTZ level to the 47.6 kcal mol^{-1} values determined at the CCSD(T) level extrapolated to the CBS. The CASPT2 energy barrier, 57.8 kcal mol^{-1}, was determined using a (14e,13o) AS and the aug-cc-pVTZ basis set. TS05 also presents a low frequency (116.08 cm^{-1}) associated to the rotation of the $CHCH_2$ group, which was treated as a 1DHR. MVK is the most stable isomer identified on the PES and was assumed as reference for the computation of the relative energy of other wells, products, and TSs. MVK can undergo keto–enol tautomerization to 2-hydroxy-1,3-butadiene (HBD) through a 64.5 kcal mol^{-1} energy barrier. The keto form (MVK) is more stable and hence favored. These results can be compared with the work of So *et al.*,[12] who focused on the ground state PES of MVK. The energy difference they calculated between the isomers HBD and MVK at the G3X-K level of theory is 9.4 kcal mol^{-1}, thus similar to the 10.0 kcal mol^{-1} here determined. So *et al.* identified two additional isomerization pathways. One is tautomerization to 1-hydroxymethylallene (barrier of 67.0 kcal mol^{-1} and endothermicity of 24.0 kcal mol^{-1} with respect to MVK) and the second is cyclization to 2-methyloxetene (barrier of 53.5 kcal mol^{-1} and endothermicity of 27.1 kcal mol^{-1} with respect to MVK).

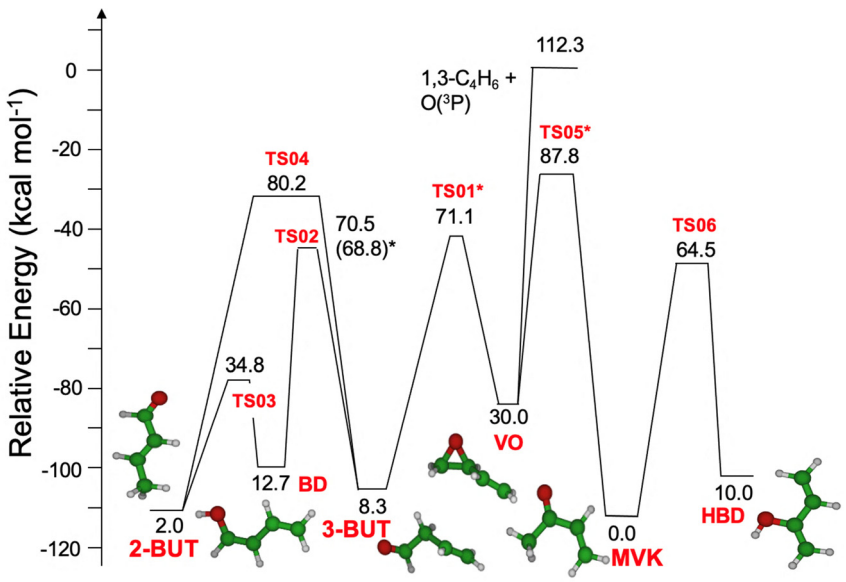

Fig. 3 Main isomerization pathways active on the singlet C_4H_6O PES, explicitly indicating the entrance channel for $O(^3P)$ addition to 1,3-C_4H_6. Energies are reported with respect to the most stable isomer, MVK. The energies of TS01 and TS05 (marked with an asterisk) were computed at the CASPT2/aug-cc-pVTZ level using the active spaces reported in Table 1. For TS02 both the CCSD(T)/CBS and CASPT2 (between parentheses) energies are reported.

These reactions were not included in the current investigation as they are significantly slower than the decomposition channels that can be accessed from MVK and the isomerization channel to HBD. This is the only relevant isomerization channel for MVK (even isomerization to VO is at least one order of magnitude slower at all temperatures and pressures included in the study), and the dominant pathway at all pressures between 500 and 1100 K.

3-BUT is the well of the PES from which the fastest decomposition channels can be accessed. It is formed by isomerization of VO through the opening of the C3 cycle and the contextual transposition of one of the hydrogen atoms from the terminal to a central carbon. From 3-BUT, direct isomerization to 2-BUT requires 71.9 kcal mol^{-1} through a single step mechanism, largely unfavored with respect to the keto–enol–keto tautomerization that connects 2- and 3-BUT. The enol form of both 3-BUT and 2-BUT is 1,3-butadien-1-ol (BD). The barrier between 3-BUT and BD is 60.5 kcal mol^{-1} when computed at the CASPT2 level and 62.2 kcal mol^{-1} at the CCSD(T)/CBS level, while enol–keto tautomerization to 2-BUT requires overcoming a small barrier of 22.1 kcal mol^{-1} with respect to BD, suggesting that, once formed, BD is rapidly converted to 2-BUT. The conversion pathway between 2- and 3-BUT here identified allows 2-BUT to access the fast decomposition pathways of 3-BUT which, as discussed in detail in Section 3.2, plays a relevant role in the decomposition 2-BUT.

It is now interesting to discuss the reactivity on the singlet C_4H_6O PES when it is accessed following the addition of O(^{3}P) to 1,3 C_4H_6. While the addition step takes place on the triplet PES, which is described in detail in our previous study,[33] a significant portion of the reactive flux reaches the singlet PES through intersystem crossing (ISC). As shown in Fig. 3, we propose that the ISC flux leads to the formation of vinyl-oxirane (VO). This is an effective description of what is a more complicated process and deserves some discussion. As mentioned, the ISC process is also described in detail in our previous study[33] of the global reactivity of 1,3-C_4H_6 with ground state oxygen O(^{3}P). There, ISC was studied theoretically and experimentally, finding its extent amounts to 67 and 66 ± 20% in the investigated experimental conditions, respectively. The major role of ISC and the active channels on the singlet PES are in line with the findings of previous works on C_4 hydrocarbons reactions with O(^{3}P), namely 1-butene[55] and 1,2-butadiene,[56] for which ISC amounted to 50% and 70%. These studies can be combined with the work of Li *et al.*[57] on ethene and ground state atomic oxygen to better understand the evolution of systems of unsaturated hydrocarbons and oxygen when ISC is active. In fact, different reaction pathways are available to the singlet diradical that is formed following ISC. It can either isomerize to oxirane (VO, in the case of 1,3-butadiene), to an aldehyde (3-BUT), to a ketone (MVK) or break into ketene and H_2. As shown in previous studies isomerization is faster than decomposition.[24,26] In addition, it can be noticed that the barrier to the formation of 3-BUT from VO is 41 kcal mol^{-1}, whereas formation of MVK from the same well requires overcoming an energy barrier of 57.8 kcal mol^{-1}. This is a consequence of the stabilization by resonance of the diradical transition state TS01 leading to 3-BUT. This suggests that the direct flux from ISC to MVK is likely smaller than that leading to VO and 3-BUT, which are then the most likely wells that can be accessed following ISC. In addition, since the only reactive pathway of VO is isomerization to 3-BUT, it is possible to further simplify the treatment of ISC by considering that it completely goes to VO, which in turn isomerizes almost uniquely to 3-BUT.

Table 2 Comparison of 0 K enthalpy changes (ΔH_0^R) from this work and ATcT

Reactants	ΔH_0^R (this work)	ΔH_0^R (ATcT)
MVK → C_2H_3 + CH_3CO	93.78	93.97 ± 0.36
MVK → C_3H_6 + CO	3.45	3.99 ± 0.26
C_3H_6 + CO → C_2H_3 + CH_3CO	90.33	89.99 ± 0.22

To validate the adopted computational approach, reaction enthalpy changes calculated at 0 K are compared with those available in the ATcT (version 1.202)[53,54] in Table 2, finding a good agreement.

3.2 Methyl vinyl ketone decomposition

The main decomposition pathways of MVK are summarized in Fig. 4. MVK can either decompose to ketene and ethylene (with barrier TS08 of 79.5 kcal mol^{-1}) or dissociate to either methyl and CH_2CHCO or vinyl and CH_3CO. Among the concerted decomposition pathways we investigated, the fastest is the one leading to the formation of C_2H_4, which can be formed directly or through isomerization to HBD and its successive fragmentation. Since TS07 has a significant T1 diagnostic of 0.063, the energy barrier was determined at the CASPT2/aug-cc-pVTZ level, using the AS described in the method section. The energy barrier of TS07 is 5.4 kcal mol^{-1} higher than that of TS08, but the vibrational frequencies of TS07 are smaller, so that both pathways contribute to this reactions channel. H loss pathways were not considered as enthalpically and entropically unfavoured with respect to the competing pathways shown in Fig. 4. The 0 K enthalpy change for the reaction leading to $CH_2C(O)CHCH_2$ + H is 95.4 kcal mol^{-1}, which makes it considerably slower than all the other reaction channels.

Rate constants for the barrierless decomposition channels were determined using VRC-TST. The decomposition of MVK to C_2H_3 and CH_3CO was studied placing a pivot point on both fragments on the radical atom and shifting them in the direction of the lobes of the breaking bond orbital, while bond fission to CH_3 and co-product included two pivot points for each fragment. Since methyl reactivity is symmetric with respect to the molecular planes, a symmetry factor of 2 was used to account for the same reactivity of each methyl hemispheric facet. The correction potentials computed for both exit channels, together with their separate contribution for geometry and level of theory corrections, are reported in Fig. 5, together with the MEP. In the case of decomposition to C_2H_3 and CH_3CO the energy correction is dominant along the whole MEP, while for the decomposition to methyl and co-product the geometry correction becomes relevant only at lower distances of the fragments,

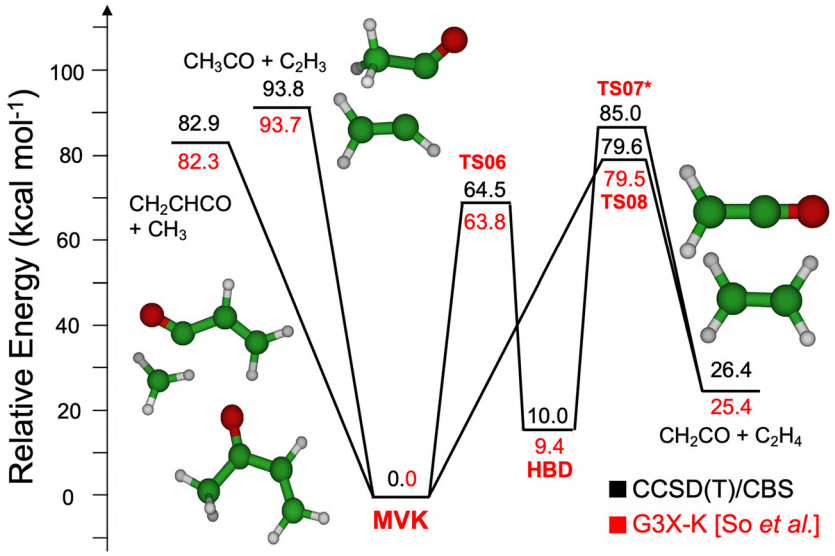

Fig. 4 Decomposition pathways of MVK and HBD. Relative energies in black refer to the results of this investigation, calculated at the CCSD(T)/CBS level, while red values are taken from literature computations carried out at the G3X-K level of theory.[12] The energy of TS07 (marked with an asterisk) was computed at the CASPT2/aug-cc-pVTZ level using the active spaces reported in Table 1.

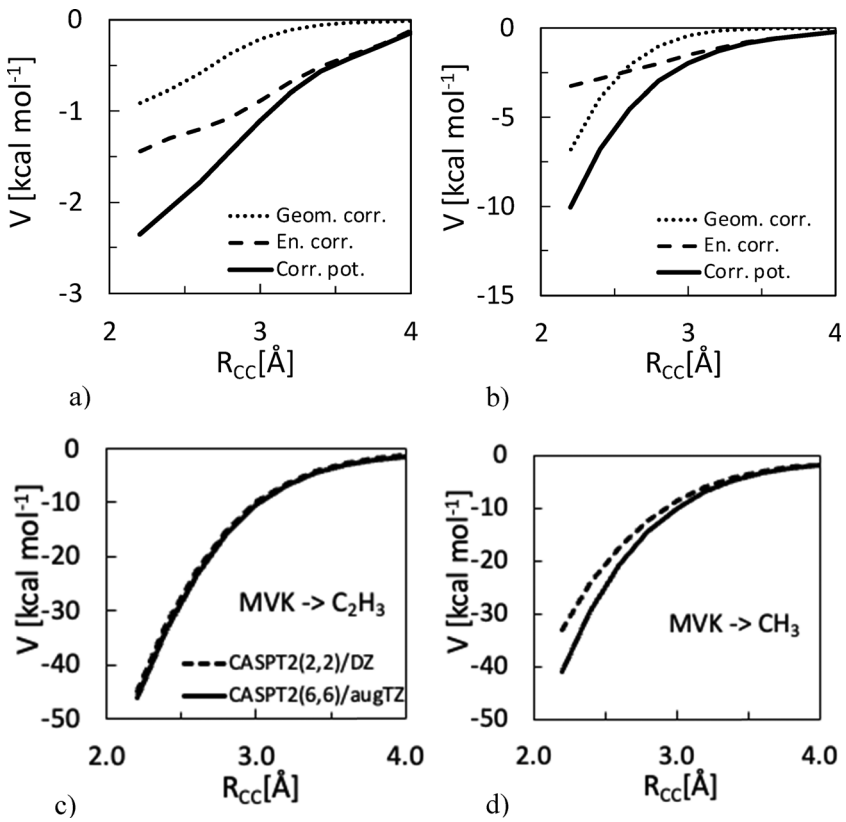

Fig. 5 Correction potential (solid), with geometry (dotted) and energy (dashed) contributions, and MEPs for decomposition of MVK to (a) and (c) C_2H_3 + CH_3CO and (b) and (d) CH_3 + CH_2CHCO.

which is expected due to the change in methyl geometry from planar (at long distances) to umbrella (at lower distances).

Fig. 6 reports the recombination rate constants calculated at the high pressure limit (HPL) as a function of the temperature. As it can be observed, the calculated rates have values comparable to the only literature reference but a more significant temperature dependence. The literature estimate for the recombination process was performed by So *et al.*,[12] who determined

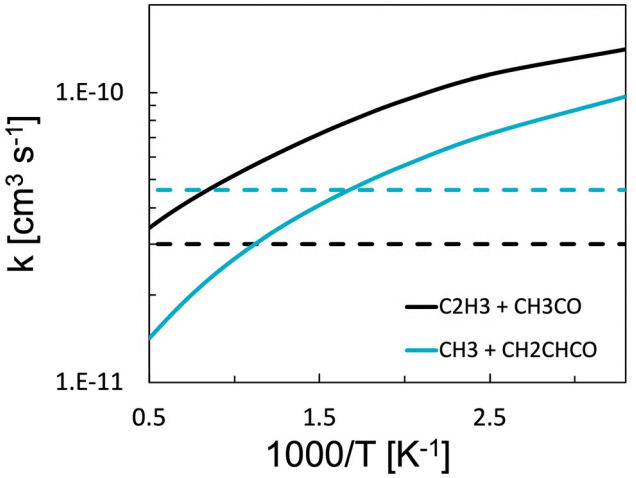

Fig. 6 HPL recombination rate constants for C_2H_3 + CH_3CO and CH_3 + CH_2CHCO to yield MVK. Solid lines represent rate constants computed in this work, dashed lines the reference values of the rate constants from So *et al.*[12]

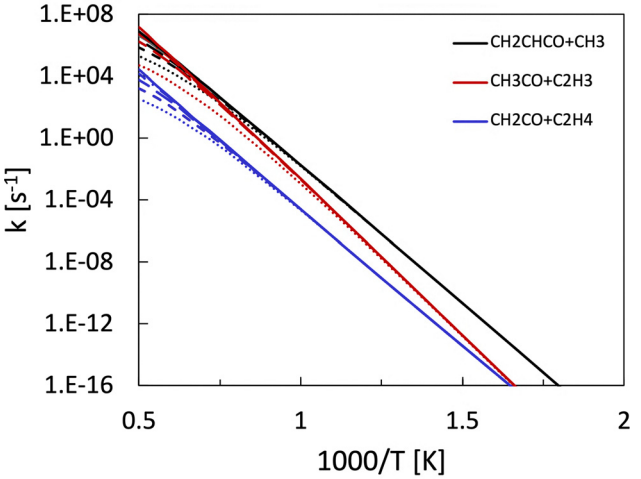

Fig. 7 Main decomposition pathways of MVK reported at the HPL (solid line) and at 0.1 atm (dotted line), 1 atm (short dash line), 10 atm (long dash line), and 100 atm (long dash – dotted line).

the HPL rate coefficients for the reverse recombination reactions selecting structurally similar reactions and the barrierless dissociation with a restricted Gorin model. In particular, MVK decomposition to vinyl and CH_3CO was approximated with the reaction $CH_3CO + C_2H_5$, whose rate was suggested by Tsang and Hampson[58] to be 3×10^{-11} cm^3 molec^{-1} s^{-1}. Similarly, the rate constant for $CH_2CHCO + CH_3$ was estimated from previous experimental studies for the reaction $CH_3CO + CH_3$. It is interesting to notice how the estimates by So *et al.* are quite reasonable, as they differ by no more than a factor of three from the present calculations, but that there is a qualitative difference between what is the dominant reaction pathway, especially at high temperatures. A comparison between the HPL rate constants for recombination for $CH_3CO + C_2H_3$ computed using VRC-TST and VTST are reported in the SI, together with a brief discussion on the shortcomings of using VTST in the RRHO approximation to determine rate constants of barrierless reactions.

Master equation simulations performed using the PES of Fig. 4 show that the two barrierless channels dominate the decomposition at all the operating conditions considered. Dissociation to CH_3 and co-product is the fastest exit channel at all pressures and up to 750 K, while at higher temperatures the production of vinyl and CH_3CO becomes significant above 1 atm. At 0.001 atm, the only important product of MVK decomposition is CH_3. The rate constants for decomposition calculated at 0.1, 1, 10 and 100 bar are compared in Fig. 7, while the calculated high pressure and PLOG rates are reported as SI.

3.3 3-Butenal decomposition

The decomposition pathways that can be accessed from the 3-BUT well play an important role in the reactivity of the singlet C_4H_6O PES. In addition to describing 3-BUT decomposition, they also describe the reactivity that follows ISC following $O(^3P)$ addition to 1,3 butadiene and contribute significantly to 2-BUT

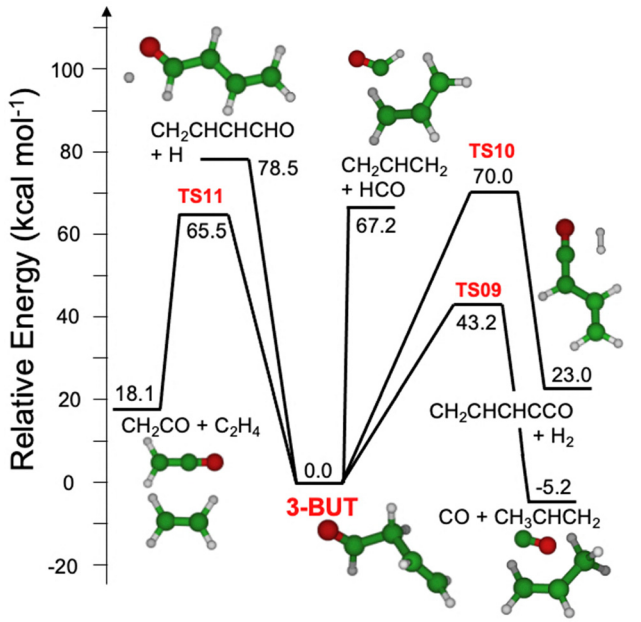

Fig. 8 Decomposition pathways of 3-BUT, taken as reference for the energies (kcal mol^{-1}).

decomposition. Fig. 8 reports the considered two barrierless exit channels and three molecular decomposition pathways. Fragmentation to HCO and CH_2CHCH_2 is favored by 11.3 kcal mol^{-1} over the loss of a hydrogen atom from the secondary carbon adjacent to the HCO group, which is the most energetically favored among the H loss channels as it leads to the formation of the resonant stabilized $CH_2CHCHCHO$ radical. Indeed, the 0 K enthalpy change for H loss from the 3-BUT acyl group, 87.8 kcal mol^{-1}, is considerably higher, while that for the barrierless decomposition channel to $CH_2CHO + C_2H_3$ is 92.4 kcal mol^{-1}, which makes both reaction pathways not competitive with those here considered. Among the bimolecular

exit channels with a barrier, decomposition to propene and CO through TS09 requires overcoming the smallest barrier with respect to the reactant, 43.2 kcal mol^{-1}. The loss of molecular hydrogen is associated to the formation of a π CO bond and a transition state, TS10, which lies at 70.0 kcal mol^{-1}, while fragmentation through TS11 to ethene and CH_2CO requires overcoming a slightly smaller energy barrier of 65.5 kcal mol^{-1}.

The rate constants for the two considered barrierless decomposition channels, to CH_2CHCH_2 + HCO and to $CH_2CHCHCHO$ + H, were computed with VRC-TST. The former was studied placing four pivot points on the allyl fragment and one on the HCO fragment, using a symmetry factor of 4 to account for the fourfold degeneracy of the resulting diving surface. The latter included a pivot point on the hydrogen atom and 2 pivot points, placed above and below the molecular plane, for $CH_2CHCHCHO$. Fig. 9 reports the computed correction potentials and MEPs for the two barrierless exit channels of 3-BUT. In both cases, the geometry correction is significant only below 2.6 Å, where the larger fragment geometries change from a planar to an out-of-plane configuration.

The recombination rates of HCO with C_3H_5 and $CH_2CHCHCHO$ with atomic hydrogen to form 3-BUT are shown in Fig. 10. It can be observed that the recombination reaction of HCO with C_3H_5, has a significant negative temperature dependence, and intersects the 2×10^{-11} cm^3 $molec^{-1}$ s^{-1} estimate of Tsang[59] at about 1000 K. The recombination of atomic hydrogen shows an inverse trend and a weaker temperature dependence, as also reported in the literature for similar processes.[60]

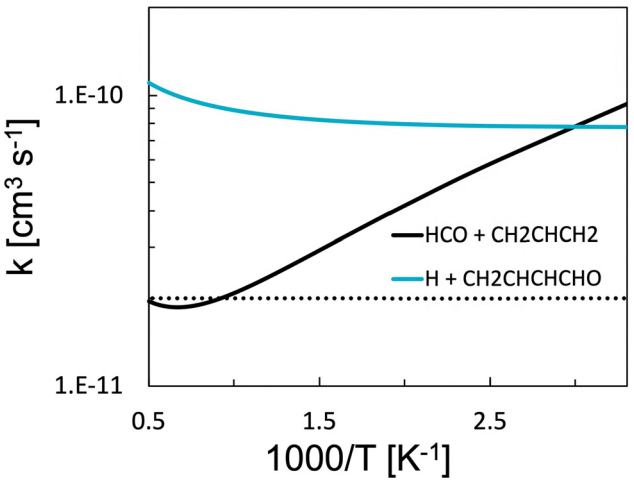

Fig. 10 HPL recombination rate constants of HCO with CH_2CHCH_2 and H with $CH_2CHCHCHO$ to form 3-BUT. The dotted line is the Tsang and Hampson[58] estimate.

The decomposition rate constants calculated at 0.1, 1, 10, and 100 atm of the main decomposition channels are reported in Fig. 11, while the calculated high pressure and PLOG rates are reported as SI. The main exit channels of the PES are molecular fragmentation to propene and CO and bond scission to HCO and CH_2CHCH_2. The former accounts for more than 95% of the reactivity at all pressures and temperatures below 900 K. Bond scission to HCO and allyl becomes competitive at

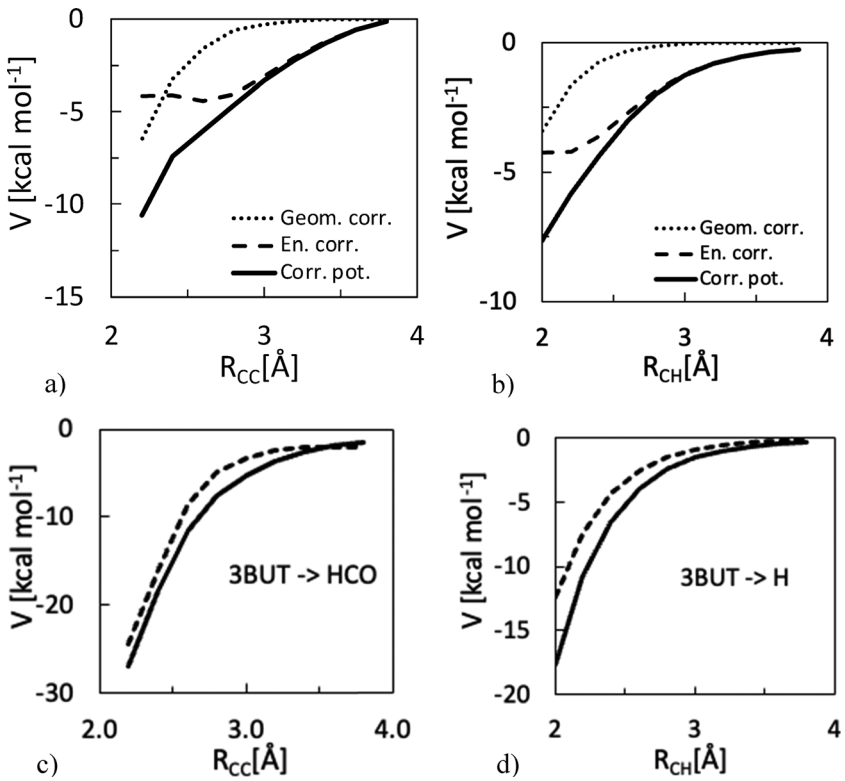

Fig. 9 Correction potentials (solid) with geometry (dotted) and energy (dashed) contributions, and MPEs for 3-BUT decomposition to (a) and (c) HCO + C_3H_5 and (b) and (d) H + $CH_2CHCHCHO$.

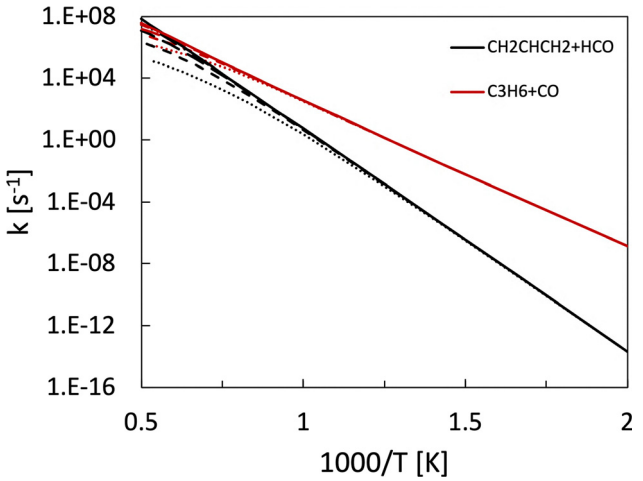

Fig. 11 Main decomposition pathways of 3-BUT reported at the HPL (solid line) and at 0.1 atm (dotted line), 1 atm (short dash line), 10 atm (long dash line), 100 atm (long dash – dotted line).

both atmospheric and high pressures and temperatures above 1200 K, while decomposition to CH_2CO and C_2H_4 is always several order of magnitudes slower. At the HPL and above 1700 K, the barrierless channel to HCO becomes dominant.

3.4 2-Butenal decomposition

The main decomposition pathways directly accessible from the 2-BUT well, reported in Fig. 12, are the three barrierless channels leading to the formation of CH_3, H, or HCO and the respective co-fragments, and the molecular pathway leading to the formation of CO and propene. The radical fragments with the lowest relative energy are atomic H and $CH_2CHCHCHO$, at

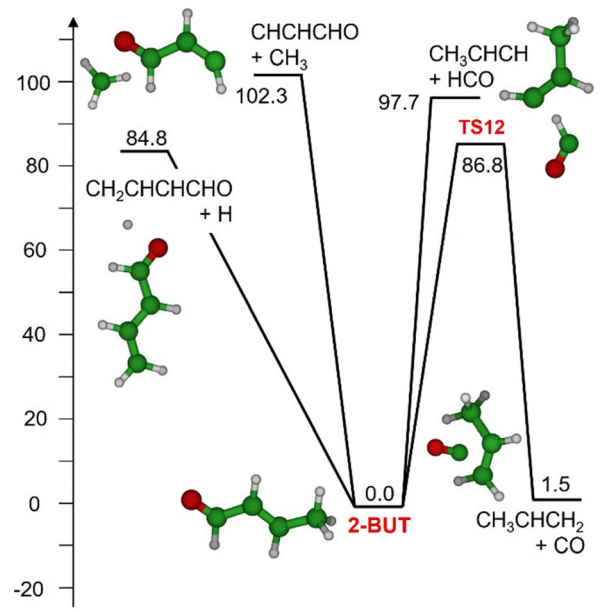

Fig. 12 Decomposition pathways of 2-BUT. The 2-butenal well is taken as reference for the calculation of relative energies (kcal mol^{-1}) for the respective reaction pathways.

84.8 kcal mol^{-1} with respect to the reactant. The other two channels require 12.9 (CH_3) and 17.5 kcal mol^{-1} (HCO) more to break the respective bonds. The considered H loss channel is the most energetically favored with respect to the others possible hydrogen bond fissions from 2-BUT, as it leads to the formation of a secondary radical stabilized by resonance. As a comparison, the 0 K enthalpy change for the relatively facile H loss from the 2-BUT acyl group, 89.2 kcal mol^{-1}, is about 4 kcal mol^{-1} higher.

The rate constants for the three considered barrierless decomposition channels were computed using VRC-TST. The bond fission to atomic hydrogen and $CH_2CHCHCHO$ was studied placing one pivot point on the hydrogen atom and two pivot points shifted from and symmetric with respect to the molecular plane for the $CH_2CHCHCHO$ fragment. Bond fission to methyl and CHCHCHO was investigated using dividing surfaces constructed using two pivot points for CH_3 and one for the other fragment, variationally shifted in the direction of the breaking bond, while for dissociation to CH_3CHCH + HCO we used one pivot point for the formyl radical and one for the CH_3CHCH fragment, both centred on the radical atom. Fig. 13 reports the contributions to the correction potentials determined for the three barrierless exit channels and the respective MEPs. In all cases, the energy contribution becomes dominant above 3 Å. The energy contribution is almost constant at different fragments distances for decomposition to methyl, while it is always relevant and monotonically increasing for the HCO channel. The geometry contribution rapidly goes to zero for all the channels considered in the study.

Fig. 14 shows the temperature dependence of all three barrierless channels at the HPL. The rate constant for the hydrogen recombination channel is almost constant and slightly increases approaching 2000 K.

The rate constants for decomposition calculated at 0.1, 1, 10 and 100 atm are reported in Fig. 15, while the calculated high pressure and PLOG rates are reported as SI.

The analysis of the decomposition pathways of 2-BUT shows that at most temperatures and pressures the main products are CO and propene. Interestingly, it can also be noticed that the phenomenological reaction rate of this channel increases with the decrease of the pressure, with the slowest rate found at the high pressure limit. While this seems counterintuitive, the motivation is that, according to the PES used for the ME simulations, decomposition to CO takes place through preliminary isomerization to 3-BUT and its successive decomposition to CO through TS09. The pressure dependence of the rate constant for this channel is therefore determined by the fact that, increasing the pressure, collisional stabilization of the wells visited before reaching TS09, which are BD and 3-BUT as shown in Fig. 3, increases of relevance. In this context, the HPL rate constant for decomposition to CO + propene of Fig. 15 is the one occurring through TS12, which is hindered by a high energy barrier of 86.8 kcal mol^{-1}. The identification of the pathway of formation of CO in 2-BUT decomposition has been the subject of some research in the literature. Erastova *et al.*[20] proposed a two-step elimination mechanism that takes place

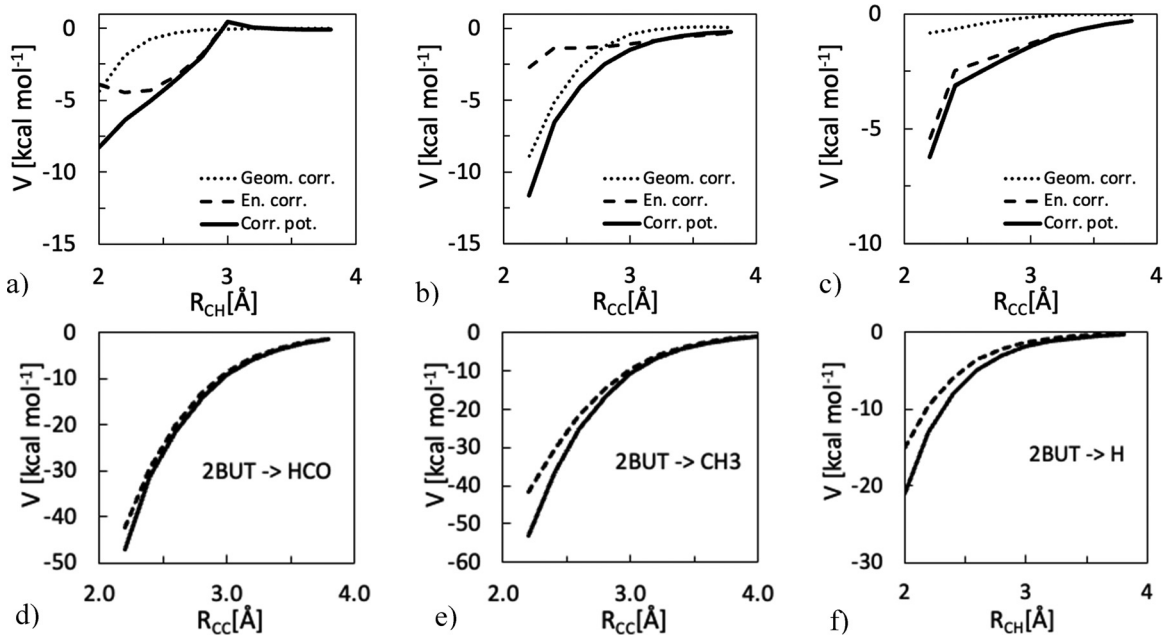

Fig. 13 Correction potential (solid), with geometry (dotted) and energy (dashed) contributions, and MEPs for decomposition of 2-BUT to (a) and (d) $CH_2CHCHCHO$ + H, (b) and (e) CH_3 + CHCHCHO, and (c) and (f) HCO + CH_3CHCH.

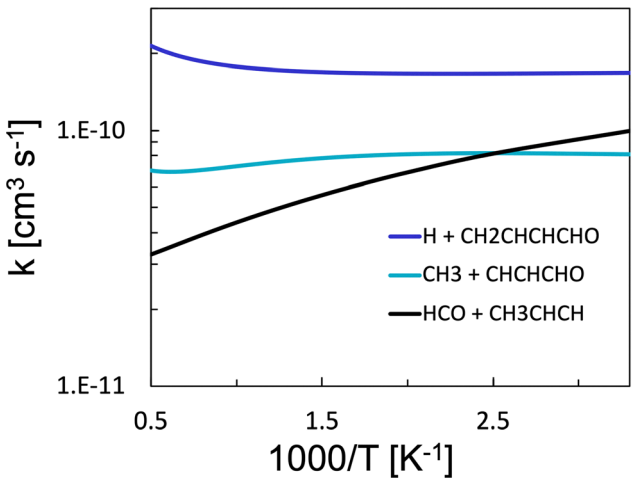

Fig. 14 Temperature dependent HPL recombination rate constants of $CH_2CHCHCHO$ + H, CH_3 + CHCHCHO, and HCO + CH_3CHCH to yield 2-BUT.

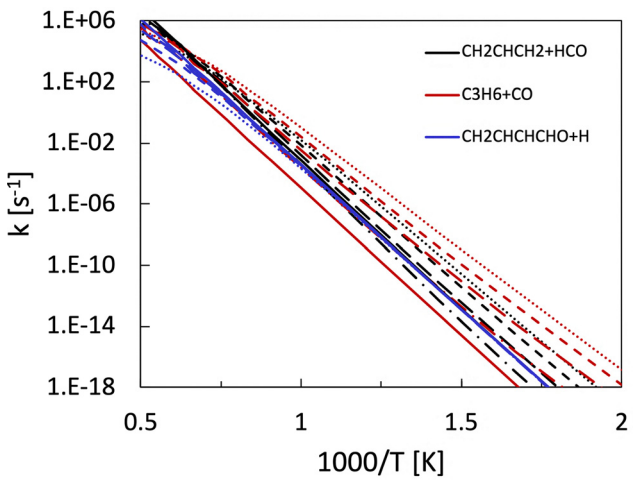

Fig. 15 Rate constants of the main decomposition pathways of 3-BUT reported at the HPL and at different pressures: 0.1 atm (dotted line), 1 atm (short dash line), 10 atm (long dash line), 100 atm (long dash – dotted line), and HPL (solid line).

though the formation of the ethylketene intermediate, followed by its decomposition to CO and propene. The energy barriers for the two isomerization steps, calculated at the B3LYP/6-31+G(d,p) level, are 76.0 and 77.3 kcal mol^{-1}, thus significantly higher than those found in this work for isomerization to 3-BUT. These high barriers for the direct decomposition of 2-BUT to propene and CO are in contrast with experimental data extrapolated from previous works.[18,61] Grela *et al.* studied the stability of the furan ring[62] as a relevant member of the family of five-membered heteroaromatic rings, which naturally occurs in coal and oil, to investigate the behavior of these compounds at high temperatures. Following this, they focused on the pyrolysis of the most important furan derivative, 2-furaldehyde, together with benzaldehyde, and 2-BUT.[61] They employed a flow reactor operated at very low pressures and slow flow rates, which allowed extrapolation to the HPL when collision with the walls was accounted for. Under these conditions, they studied the extent of decomposition of 2-BUT as a function of temperature, between 1040 and 1180 K. Lifshitz *et al.*[18] also investigated the reactivity of 2-BUT, as a major product of 2,3-dihydrofuran pyrolysis. They commented on the absence of

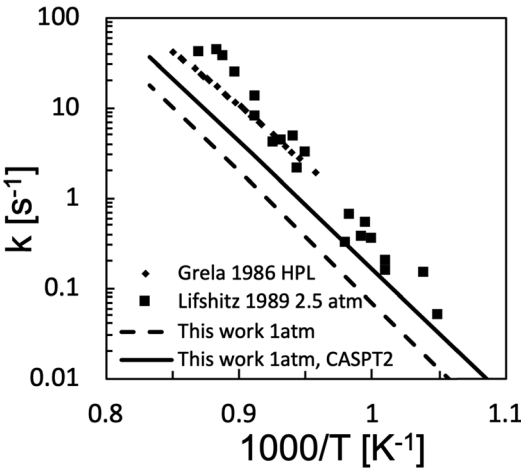

Fig. 16 Comparison of the calculated decomposition rate of 2-BUT to CO with the experimental measurements of Grela *et al.*[61] (diamonds) and Lifshitz *et al.*[18] (squares). Rate constants determined in this work were computed with the energy barrier of TS02 evaluated at the CASPT2 (continuous line) and the CCSD(T)/CBS (dashed line) levels of theory by solving the ME over the full PES to determine phenomenological rate constants and accounting for reaction fluxes coming from all wells.

other products in the study conducted by Grela *et al.*[61] and prepared an experimental set-up to investigate the products distribution of the unimolecular decomposition 2-BUT. They employed reflected shocks in a single pulse shock tube reactor to study the pyrolysis of 0.5% crotonaldehyde in Ar between 987 and 1353 K. CO is the major product over the whole temperature range, together with C_2H_2, whose concentration is around half of that of CO over most temperatures investigated. Other relevant products (the ratio of their concentration with respect to the major product CO is always less than 25%) are CH_4, C_2H_4 (at higher temperatures), and C_3H_6. To compare the results of the present calculations with the experimental CO measurements of Grela *et al.* and Lifshitz *et al.* it is necessary to account for the reaction fluxes coming from 2-BUT, as well as from the wells that can be accessed through isomerization from 2-BUT in the investigated operating conditions and have phenomenological rates leading to CO, which are mostly BD and 3-BUT. To do that it is necessary to know the relative concentration of both BD and 3-BUT with respect to 2-BUT, which can either be determined through integration of the phenomenological rates computed by MESS, or assuming that BD and 3-BUT reach rapidly a steady state concentration. In the present work we used the second approach, which allowed to compute the rate of CO formation reported in Fig. 16, where it is compared with the available experimental data. The calculated decomposition rates are sensitive to the TS02 energy barrier, with the experimental data being underestimated by the present calculations by a factor of 2–3 when using CASPT2 energies and by a factor of 4–5 when using CCSD(T) energies. The underestimation of the experimental data may be due to several reasons, among which the main are: (i) the contribution of secondary reactivity, and in particular of radical chain pathways; (ii) the existence of an alternative decomposition channel; (iii) an overestimation of the energy barrier of TS02. In particular it would be possible to fit experimental data well if the energy barrier of TS02 is lowered by about 1 kcal mol^{-1} with respect to the value calculated at the CASPT2 level. It should though be noted that in the investigated temperature and pressure ranges the calculated rate of decomposition to HCO + C_3H_5 is about 10% of that of decomposition to CO and C_3H_6. As HCO will rapidly decompose to H and CO, it follows that this channel will lead to the formation of a considerable concentration of radical species, which may accelerate relevantly the 2-BUT reactivity, thus motivating the observed underestimation of the experimental data.

4. Conclusions

This work focused on the study of the reactivity on the C_4H_6O singlet state PES by means of high-level theoretical calculations. The theoretical investigation of a singlet state PES poses different challenges, which were addressed by employing both single and multireference approaches aided by the EStokTP software, and by relying on the VRC-TST theoretical framework to study barrierless exit channels. In particular, VRC-TST was applied with a semi-automated procedure implemented in EStokTP to calculate rate constants for the recombination of seven barrierless channels. The procedure involved the computation of a correction potential along the MEP of each barrierless channel and the preparation of the input files for the VRC-TST software VaReCoF. Multireference methods were used to sample stochastically the PES in VRC-TST simulations, and the only manual interventions required were due to checks of the consistency of the AS automatically selected throughout the protocol. The novel semi-automated procedure we implemented in EStokTP was successful in computing the correction potential for all seven barrierless exit channels. For these, rate constants were obtained through master equation simulations and are reported in the SI in PLOG form, for perspective successive use in kinetic simulations. Temperature dependent recombination rate constants were also derived for the investigated barrierless channels, which had previously not been determined at this level of theory in the literature.

The main decomposition pathways from the three most stable isomers on the C_4H_6O PES, namely MVK, 2-BUT and 3-BUT, were then studied. Rate constant of the main isomerization channels were determined using both single reference methods as well as multireference approaches to determine energy barriers of saddle points having bi-radical nature. A new mechanism for the decomposition of 2-BUT to CO and propene was proposed, which involves isomerization to 3-BUT through an enol intermediate. The calculated rate of formation of CO underestimates experimental data by a factor comprised between 2 and 5, depending on the level of theory at which the energy barrier for the isomerization step is computed. The disagreement may be determined either by the impact of secondary chemistry, as it is found that radical formation pathways are active parallel to CO decomposition at relevant rates, or to an underestimation of the calculated energy barrier.

It would be useful to address this point through successive studies in which kinetic simulations are used to interpret experimental measurements. The rate constants computed in this work, reported in the SI in the PLOG format in ample temperature and pressure ranges, provide a useful resource both to further investigate the systems here studied, as well as to be included in kinetic mechanisms dedicated to the study of the reactivity of biofuels in which unsaturated aldehydes and ketones may appear as intermediate species.

Conflicts of interest

There are no conflicts to declare.

Data availability

The data supporting this article have been included as part of the SI. Supplementary information: Arrhenius fits of calculated rate constants in PLOG format and comparison of VTST and VRC-TST rate constants; MESS input files are reported in tar attachment. See DOI: https://doi.org/10.1039/d5cp01744k.

Acknowledgements

We acknowledge financial support under the National Recovery and Resilience Plan (NRRP), Mission 4, Component 2, Investment 1.1, Call for tender no. 1409 published on 14.9.2022 by the Italian Ministry of University and Research (MUR), funded by the European Union – NextGenerationEU – Project Title: GasChem4Air – PRIN Grant Number P2022ZFNBL – Grant Assignment Decree No. 1386 adopted on 28-12-2023 by the Italian Ministry of University and Research (MUR).

References

1 B. Yang, W. Sun, K. Moshammer and N. Hansen, Review of the Influence of Oxygenated Additives on the Combustion Chemistry of Hydrocarbons, *Energy Fuels*, 2021, **35**, 13550–13568.
2 Z. Liu, X. Fan, H. Chen, Q. Hou, H. Liao, J. Yang, L. Zhao, F. Zhang and B. Yang, Characterization of the low-temperature oxidation chemistry of an unsaturated aldehyde 2-butenal in a Jet-stirred reactor, *Proc. Combust. Inst.*, 2023, **39**, 435–444.
3 M. Pelucchi, C. Cavallotti, E. Ranzi, A. Frassoldati and T. Faravelli, Relative Reactivity of Oxygenated Fuels: Alcohols, Aldehydes, Ketones, and Methyl Esters, *Energy Fuels*, 2016, **30**, 8665–8679.
4 G. Eerdekens, L. Ganzeveld, J. Vilà-Guerau de Arellano, T. Klüpfel, V. Sinha, N. Yassaa, J. Williams, H. Harder, D. Kubistin, M. Martinez and J. Lelieveld, Flux estimates of isoprene, methanol and acetone from airborne PTR-MS measurements over the tropical rainforest during the GABRIEL 2005 campaign, *J. Atmos. Chem. Phys.*, 2009, **9**, 4207–4227.
5 J. P. Porterfield, T. L. Nguyen, J. H. Baraban, G. T. Buckingham, T. P. Troy, O. Kostko, M. Ahmed, J. F. Stanton, J. W. Daily and G. B. Ellison, Isomerization and Fragmentation of Cyclohexanone in a Heated Micro-Reactor, *J. Phys. Chem. A*, 2015, **119**(51), 12635–12647.
6 A. Tajti, P. G. Szalay, A. G. Császár, M. Kállay, J. Gauss, E. F. Valeev, B. A. Flowers, J. Vázquez and J. F. Stanton, HEAT: High Accuracy Extrapolated *Ab Initio* Thermochemistry, *J. Chem. Phys.*, 2004, **121**(23), 11599–11613.
7 Y. J. Bomble, J. Vázquez, M. Kállay, C. Michauk, P. G. Szalay, A. G. Császár, J. Gauss and J. F. Stanton, High-Accuracy Extrapolated *Ab Initio* Thermochemistry. II. Minor Improvements to the Protocol and a Vital Simplification, *J. Chem. Phys.*, 2006, **125**(6), 064108.
8 M. E. Harding, J. Vázquez, B. Ruscic, A. K. Wilson, J. Gauss and J. F. Stanton, High-Accuracy Extrapolated *Ab Initio* Thermochemistry. III. Additional Improvements and Overview, *J. Chem. Phys.*, 2008, **128**(11), 114111.
9 F. Tureček, 2-Hydroxybutadiene: Preparation, Ionization Energy and Heat of Formation, *Tetrahedron Lett.*, 1984, **25**(45), 5133–5134.
10 C. A. Taatjes, N. Hansen, A. McIlroy, J. A. Miller, J. P. Senosiain, S. J. Klippenstein, F. Qi, L. Sheng, Y. Zhang, T. A. Cool, J. Wang, P. R. Westmoreland, M. E. Law, T. Kasper and K. Kohse-Höinghaus, Enols Are Common Intermediates in Hydrocarbon Oxidation, *Science*, 2005, **308**(5730), 1887–1889.
11 D. E. Couch, Q. L. D. Nguyen, A. Liu, D. D. Hickstein, H. C. Kapteyn, M. M. Murnane and N. J. Labbe, Detection of the Keto-Enol Tautomerization in Acetaldehyde, Acetone, Cyclohexanone, and Methyl Vinyl Ketone with a Novel VUV Light Source, *Proc. Combust. Inst.*, 2021, **38**(1), 1737–1744.
12 S. So, U. Wille and G. da Silva, Photoisomerization of Methyl Vinyl Ketone and Methacrolein in the Troposphere: A Theoretical Investigation of Ground-State Reaction Pathways, *ACS Earth Space Chem.*, 2018, **2**(8), 753–763.
13 K. Hoyermann, S. Maarfeld, F. Nacke, J. Nothdurft, M. Olzmann, J. Wehmeyer, O. Welz and T. Zeuch, Rate Coefficients for Cycloalkyl + O Reactions and Product Branching in the Decomposition of Chemically Activated Cycloalkoxy Radicals: An Experimental and Theoretical Study, *Phys. Chem. Chem. Phys.*, 2010, **12**(31), 8953.
14 Z. Tian, T. Yuan, R. Fournet, P.-A. Glaude, B. Sirjean, F. Battin-Leclerc, K. Zhang and F. Qi, An Experimental and Kinetic Investigation of Premixed Furan/Oxygen/Argon Flames, *Combust. Flame*, 2011, **158**(4), 756–773.
15 Y. Fenard, H. Song, H. Minwegen, P. Parab, C. Sampaio Mergulhão, G. Vanhove and K.-A. Heufer, 2,5-Dimethyltetrahydrofuran Combustion: Ignition Delay Times at High and Low Temperatures, Speciation Measurements and Detailed Kinetic Modeling, *Combust. Flame*, 2019, **203**, 341–351.
16 R. G. Butler and I. Glassman, Cyclopentadiene Combustion in a Plug Flow Reactor near 1150K, *Proc. Combust. Inst.*, 2009, **32**(1), 395–402.
17 M. Bertero, G. de la Puente and U. Sedran, Fuels from Bio-Oils: Bio-Oil Production from Different Residual Sources,

Characterization and Thermal Conditioning, *Fuel*, 2012, **95**, 263–271.

18 A. Lifshitz, M. Bidani and C. Tamburu, Decomposition of Crotonaldehyde at Elevated Temperatures: Studies with a Single-Pulse Shock Tube, *J. Phys. Chem.*, 1989, **93**(20), 7161–7165.

19 O. Y. Chabán, R. M. Domínguez, A. Herize, M. Tosta, A. Cuenca and G. Chuchani, Kinetic and Mechanism of the Homogeneous, Unimolecular Elimination Of α,β-Unsaturated Aldehydes in the Gas Phase, *J. Phys. Org. Chem.*, 2007, **20**(5), 307–312.

20 V. Erastova, J. Rodríguez-Otero, E. M. Cabaleiro-Lago and Á. Peña-Gallego, A Computational Study of the Mechanism of the Unimolecular Elimination of α,β-Unsaturated Aldehydes in the Gas Phase, *J. Mol. Model.*, 2011, **17**(1), 21–26.

21 Y. Fathi and G. Meloni, Study of the Synchrotron Photoionization Oxidation of 2-Methylfuran Initiated by $O(^3P)$ under Low-Temperature Conditions at 550 and 650 K, *J. Phys. Chem. A*, 2017, **121**(37), 6966–6980.

22 M. O. Passos, I. A. Lins, M. F. Venâncio and T. V. Alves, Differences in the Torsional Anharmonicity between Reactant and Transition State: The Case of 3-Butenal + H Abstraction Reactions, *Phys. Chem. Chem. Phys.*, 2021, **23**(44), 25414–25423.

23 R. J. Cvetanović, Evaluated Chemical Kinetic Data for the Reactions of Atomic Oxygen $O(^3P)$ with Unsaturated Hydrocarbons, *J. Phys. Chem. Ref. Data*, 1987, **16**(2), 261–326.

24 C. Cavallotti, F. Leonori, N. Balucani, V. Nevrly, A. Bergeat, S. Falcinelli, G. Vanuzzo and P. Casavecchia, Relevance of the Channel Leading to Formaldehyde + Triplet Ethylidene in the $O(^3P)$ + Propene Reaction under Combustion Conditions, *J. Phys. Chem. Lett.*, 2014, **5**(23), 4213–4218.

25 F. Leonori, N. Balucani, V. Nevrly, A. Bergeat, S. Falcinelli, G. Vanuzzo, P. Casavecchia and C. Cavallotti, Experimental and Theoretical Studies on the Dynamics of the $O(^3P)$ + Propene Reaction: Primary Products, Branching Ratios, and Role of Intersystem Crossing, *J. Phys. Chem. C*, 2015, **119**(26), 14632–14652.

26 I. Gimondi, C. Cavallotti, G. Vanuzzo, N. Balucani and P. Casavecchia, Reaction Dynamics of $O(^3P)$ + Propyne: II. Primary Products, Branching Ratios, and Role of Intersystem Crossing from Ab Initio Coupled Triplet/Singlet Potential Energy Surfaces and Statistical Calculations, *J. Phys. Chem. A*, 2016, **120**(27), 4619–4633.

27 L. Pratali Maffei, C. Cavallotti, A. Caracciolo, N. Balucani and P. Casavecchia, Rate Rules for the Reactions of Oxygen Atoms with Terminal Alkenes, *Fuel*, 2020, **263**, 116536.

28 C. Cavallotti, C. De Falco, L. Pratali Maffei, A. Caracciolo, G. Vanuzzo, N. Balucani and P. Casavecchia, Theoretical Study of the Extent of Intersystem Crossing in the $O(^3P)$ + C_6H_6 Reaction with Experimental Validation, *J. Phys. Chem. Lett.*, 2020, **11**(22), 9621–9628.

29 G. Vanuzzo, A. Caracciolo, T. K. Minton, N. Balucani, P. Casavecchia, C. de Falco, A. Baggioli and C. Cavallotti, Crossed-Beam and Theoretical Studies of the $O(^3P,^1D)$ + Benzene Reactions: Primary Products, Branching Fractions, and Role of Intersystem Crossing, *J. Phys. Chem. A*, 2021, **125**(38), 8434–8453.

30 P. Recio, S. Alessandrini, G. Vanuzzo, G. Pannacci, A. Baggioli, D. Marchione, A. Caracciolo, V. J. Murray, P. Casavecchia, N. Balucani, C. Cavallotti, C. Puzzarini and V. Barone, Intersystem Crossing in the Entrance Channel of the Reaction of O(3P) with Pyridine, *Nat. Chem.*, 2022, **14**, 1405–1412.

31 G. Yin, X. Lv, E. Hu, B. Xiao, H. Shen and Z. Huang, Experimental and Chemical Kinetic Study on the Low Temperature Oxidation of 1,3-Butadiene in a Jet-Stirred Reactor, *Fuel*, 2022, **315**, 123168.

32 P. Dagaut and M. Cathonnet, The Oxidation of 1,3-Butadiene: Experimental Results and Kinetic Modeling, *Combust. Sci. Technol.*, 1998, **140**(1–6), 225–257.

33 C. Cavallotti, A. Della Libera, C.-W. Zhou, P. Recio, A. Caracciolo, N. Balucani and P. Casavecchia, Crossed-Beam and Theoretical Studies of Multichannel Nonadiabatic Reactions: Branching Fractions and Role of Intersystem Crossing for $O(^3P)$ + 1,3-Butadiene, *Faraday Discuss.*, 2022, **238**, 161–182.

34 S. J. Klippenstein and C. Cavallotti, Ab Initio Kinetics for Pyrolysis and Combustion Systems, *Computer Aided Chemical Engineering*, Elsevier, 2019, vol. 45, pp. 115–167.

35 S. J. Klippenstein, From Theoretical Reaction Dynamics to Chemical Modeling of Combustion, *Proc. Combust. Inst.*, 2017, **36**(1), 77–111.

36 C. Cavallotti, Automation of chemical kinetics: Status and challenges, *Proc. Combust. Inst.*, 2023, **39**, 1–18.

37 R. Van de Vijver and J. Zádor, KinBot: Automated Stationary Point Search on Potential Energy Surfaces, *Comput. Phys. Commun.*, 2020, **248**, 106947.

38 S. Maeda, K. Ohno and K. Morokuma, Systematic Exploration of the Mechanism of Chemical Reactions: The Global Reaction Route Mapping (GRRM) Strategy Using the ADDF and AFIR Methods, *Phys. Chem. Chem. Phys.*, 2013, **15**(11), 3683.

39 P. Zimmerman, Reliable Transition State Searches Integrated with the Growing String Method, *J. Chem. Theory Comput.*, 2013, **9**(7), 3043–3050.

40 C. A. Grambow, A. Jamal, Y.-P. Li, W. H. Green, J. Zádor and Y. V. Suleimanov, Unimolecular Reaction Pathways of a γ-Ketohydroperoxide from Combined Application of Automated Reaction Discovery Methods, *J. Am. Chem. Soc.*, 2018, **140**(3), 1035–1048.

41 Y. Georgievskii and S. J. Klippenstein, Transition State Theory for Multichannel Addition Reactions: Multifaceted Dividing Surfaces, *J. Phys. Chem. A*, 2003, **107**(46), 9776–9781.

42 Y. Georgievskii, J. A. Miller and S. J. Klippenstein, Association Rate Constants for Reactions between Resonance-Stabilized Radicals: C3H3 + C3H3, C3H3 + C3H5, and C3H5 + C3H5, *Phys. Chem. Chem. Phys.*, 2007, **9**(31), 4259.

43 C. Cavallotti, M. Pelucchi, Y. Georgievskii and S. J. Klippenstein, EStokTP: Electronic Structure to Temperature- and Pressure-Dependent Rate Constants—A Code for Automatically Predicting the Thermal Kinetics of Reactions, *J. Chem. Theory Comput.*, 2019, **15**(2), 1122–1145.

44 J. M. L. Martin, Ab Initio Total Atomization Energies of Small Molecules—towards the Basis Set Limit, *Chem. Phys. Lett.*, 1996, **259**(5–6), 669–678.
45 Y. Georgievskii, J. A. Miller, M. P. Burke and S. J. Klippenstein, Reformulation and Solution of the Master Equation for Multiple-Well Chemical Reactions, *J. Phys. Chem. A*, 2013, **117**(46), 12146–12154.
46 A. W. Jasper, ''Third-body'' Collision Parameters for Hydrocarbons, Alcohols, and Hydroperoxides and an Effective Internal Rotor Approach for Estimating Them, *Int. J. Chem. Kinet.*, 2020, **52**(6), 387–402.
47 J. Lupi, C. Puzzarini, C. Cavallotti and V. Barone, State-of-the-Art Quantum Chemistry Meets Variable Reaction Coordinate Transition State Theory to Solve the Puzzling Case of the H_2S + Cl System, *J. Chem. Theory Comput.*, 2020, **16**(8), 5090–5104.
48 L. B. Harding, Y. Georgievskii and S. J. Klippenstein, Predictive Theory for Hydrogen Atom – Hydrocarbon Radical Association Kinetics, *J. Phys. Chem. A*, 2005, **109**, 4646–4656.
49 Y. Georgievskii, L. B. Harding and S. J. Klippenstein, VaReCoF 2016.3.23, available at **https://tcg.cse.anl.gov/papr/codes/varecof.html**.
50 H.-J. Werner, P. J. Knowles, G. Knizia, F. R. Manby and M. Schütz, Molpro: A General-Purpose Quantum Chemistry Program Package, *Wiley Interdiscip. Rev.:Comput. Mol. Sci.*, 2012, **2**(2), 242–253.
51 H.-J. Werner, P. J. Knowles, F. R. Manby, J. A. Black, K. Doll, A. Heßelmann, D. Kats, A. Köhn, T. Korona, D. A. Kreplin, Q. Ma, T. F. Miller, A. Mitrushchenkov, K. A. Peterson, I. Polyak, G. Rauhut and M. Sibaev, The Molpro Quantum Chemistry Package, *J. Chem. Phys.*, 2020, **152**(14), 144107.
52 L. Pratali Maffei, M. Pelucchi, C. Cavallotti, A. Bertolino and T. Faravelli, Master equation lumping for multi-well potential energy surfaces: A bridge between ab initio based rate constant calculations and large kinetic mechanisms, *Chem. Eng. J.*, 2021, **422**, 129954.
53 B. Ruscic Active Thermochemical Tables, Version 1.202. **https://atct.anl.gov/** Accessed May 5, 2025.
54 B. Ruscic, R. E. Pinzon, M. L. Morton, G. von Laszewski, S. Bittner, S. G. Nijsure, K. A. Amin, M. Minkoff and A. F. Wagner, Introduction to Active Thermochemical Tables: Several ''Key'' Enthalpies of Formation Revisited, *J. Phys. Chem. A*, 2004, **108**, 9979–9997.
55 A. Caracciolo, G. Vanuzzo, N. Balucani, D. Stranges, P. Casavecchia, L. Pratali Maffei and C. Cavallotti, Combined Experimental and Theoretical Studies of the $O(^3P)$ + 1-Butene Reaction Dynamics: Primary Products, Branching Fractions, and Role of Intersystem Crossing, *J. Phys. Chem. A*, 2019, **123**(46), 9934–9956.
56 A. Caracciolo, G. Vanuzzo, N. Balucani, D. Stranges, S. Tanteri, C. Cavallotti and P. Casavecchia, Crossed Molecular Beams and Theoretical Studies of the $O(^3P)$+ 1,2-Butadiene Reaction: Dominant Formation of propene + CO and Ethylidene + ketene Molecular Channels, *Chin. J. Chem. Phys.*, 2019, **32**(1), 113–122.
57 X. Li, A. W. Jasper, J. Zádor, J. A. Miller and S. J. Klippenstein, Theoretical Kinetics of O+ C_2H_4, *Proc. Combust. Inst.*, 2017, **36**(1), 219–227.
58 W. Tsang and R. F. Hampson, Chemical Kinetic Data Base for Combustion Chemistry. Part I. Methane and Related Compounds, *J. Phys. Chem. Ref. Data*, 1986, **15**(3), 1087–1279.
59 W. Tsang, Chemical Kinetic Data Base for Combustion Chemistry. Part V. Propene, *J. Phys. Chem. Ref. Data*, 1991, **20**(2), 221–273.
60 L. B. Harding, S. J. Klippenstein and Y. Georgievskii, On the Combination Reactions of Hydrogen Atoms with Resonance-Stabilized Hydrocarbon Radicals, *J. Phys. Chem. A*, 2007, **111**(19), 3789–3801.
61 M. A. Grela and A. J. Colussi, Kinetics and Mechanism of the Thermal Decomposition of Unsaturated Aldehydes: Benzaldehyde, 2-Butenal, and 2-Furaldehyde, *J. Phys. Chem.*, 1986, **90**(3), 434–437.
62 M. A. Grela, V. T. Amorebieta and A. J. Colussi, Very Low Pressure Pyrolysis of Furan, 2-Methylfuran and 2,5-Dimethylfuran. The Stability of the Furan Ring, *J. Phys. Chem.*, 1985, **89**(1), 38–41.